Journal of Research in Health Sciences
ISSN: 2228-7809 | https://jrhsjournal.com

Dynamic and Structural Behaviour of Fullerene Encapsulation within an Adaptable Supramolecular Host

Dr. Lukas Schneider[1]*, Dr. Anna Weber[1], Dr. Jonas Bauer[2], Dr. Clara Hoffmann[2], Dr. Felix Krüger[3], Dr. Sophie Lang[3]
[1]Charité – Universitätsmedizin Berlin, Berlin, Germany
[2]University Hospital Heidelberg, Heidelberg, Germany
[3]Ludwig Maximilian University Hospital, Munich, Germany

ABSTRACT: The dynamic adaptability of tetragonal prismatic nanocapsule $\mathbf{1}^{8+}$ in the selective separation of fullerenes and endohedral metallofullerenes (EMFs) remains unexplored. Therefore, the essential molecular details of the fullerene recognition and binding process into the coordination capsule and the origins of fullerene selectivity remain elusive. In this work, the key steps of fullerene recognition and binding processes have been deciphered by designing a protocol which combines ^{1}H-^{1}H exchange spectroscopy (2D-EXSY) NMR experiments, long time-scale Molecular Dynamics (MD) and accelerated Molecular Dynamics (aMD) simulations, which are combined to completely reconstruct the spontaneous binding and unbinding pathways from nanosecond to second time-range. On one hand, binding (k'_{on}) and unbinding (k_{off}) rate constants were extracted from ^{1}H-^{1}H exchange spectroscopy (EXSY) NMR experiments for both C_{60} and C_{70}. On the other hand, MD and aMD allowed monitoring the molecular basis of the encapsulation and guest competition processes at a very early stage under non-equilibrium conditions, displaying dynamical adaptability features similar to those observed in the process of biomolecular recognition in proteins. In addition, the encapsulation of azafullerene $(C_{59}N)_2$ within a supramolecular coordination capsule has been studied for the first time, showcasing the pros and cons of the dumbbell-shaped in the dynamics of the encapsulation process and in the stability of the final bound adduct. The powerful combination of NMR, MD, and aMD methodologies allows to obtain a precise picture of the subtle events directing the encapsulation, and is thus a predictive tool for understanding host-guest encapsulation and interactions in numerous supramolecular systems.

INTRODUCTION

Molecular recognition is a key concept in biology and chemistry.[1-3] The network and stability of non-covalent interactions established between the binding partners and the flexibility of the interacting molecules determines the temporary nature of the complex formed. The mechanisms through which molecules interplay to attain stable (and often transient) states are complex and involve a series of interconnected intermediate, misbound, and transition states. The pathways that drive recognition and dissociation are strongly influenced by the dynamism of the interacting partners. Large molecules exist as dynamic conformational ensembles and their ability to adopt different conformations play a key role along the molecular recognition process.[4] The motions required to switch between different conformations occur at a variety of timescales that can facilitate or hinder binding and unbinding processes. The rates of interconversion between different conformations and their relative populations can change upon binding and be altered by the nature of the guest. By unravelling the dynamic details of association and dissociation pathways it is possible to gain insight into the detailed molecular mechanisms of relevant chemical processes and, then, to harness this information to enhance the rational design of novel drugs, protein assemblies, and supramolecular complexes.

Many fascinating supramolecular host-guest systems have been reported in the last decades.[5-8] In the vast majority of these reports, only the host-guest adducts formed are under the spotlight. These adducts have been fully characterized in the solid state by means of X-ray diffraction and in solution by NMR and other spectroscopic techniques.[9-10] However, due to the static picture given by crystallography and the chemical shift time-scale resolution (seconds to ms) of NMR, an oversimplified picture of the binding and unbinding processes is obtained, thus the understanding of the fundamental molecular and dynamical aspects guiding the initial steps of supramolecular host-guest recognition remains in the dark. In order to design a substrate-selective receptor molecule it is imperative to precisely understand the dynamical steps and conformational changes in which the receptor recognizes, interacts and selectively binds to a certain substrate under non-equilibrium conditions. Tuning recognition pathways and the plasticity and dynamics of the host offers new routes towards improving rational design of supramolecular plataforms.[11]

Molecular dynamics (MD) simulations represent a reliable tool for describing the intrinsic conformational dynamics, the binding pathways and binding modes of a host-guest system in solution at the atomic level.[12-15] MD simulations have been vastly used to characterize step by step the molecular basis of intricate drug binding and unbinding pathways in biological systems.[16-22] In the field of supramolecular chemistry the number of examples studying recognition pathways of host-guest binding and self-assembly in non-equilibrium conditions are scarce.[11, 23-29] Applications of MD simulations are in general focused to characterize the intrinsic dynamics of the bound complex,[30]to estimate free energies of binding,[31] or as a benchmark for force-field calibration.[32] During the past several years, many short-time scale MD simulations of cyclodextrins or crown-ethers and their inclusion complexes have been reported.[33-34] MD simulations of host-guest adducts have also been combined with quantum chemistry tools for predicting supramolecular catalysis in metallocages and cavitands.[35-38]

However, in general, a tremendous amount of conformational sampling is required to reach timescales of interest in supramolecular chemistry. For example, common guests exchange in the milliseconds to seconds time scale making this process a rare event. These timescales are still not accessible for studying spontaneous binding and exchange of multiple guests with

unbiased MD simulations.[39] In addition, for intrinsically dynamic hosts, complex guests, and for systems where multiple binding pathways exist is complicated to capture all events with a collective variable without exploring *a priori* the unconstrained binding and unbinding pathways.[40-41] Accelerated molecular dynamics (aMD),[42-43] a versatile enhanced sampling technique that speeds up molecular dynamics and does not rely on the *a priori* definition of reaction coordinates allows for an unguided sampling of spontaneous binding and unbinding events, capturing all the essential details of these processes.[44-45] A combination of MD and aMD can be used as a tool to mimic a computational nanoreactor to characterize step by step the dynamics, spontaneous binding, and competition between multiple guests in supramolecular host-guest adducts.

Herein, a tandem protocol has been developed, which combines 2D ^{1}H-^{1}H exchange (EXSY) NMR spectroscopy with MD-based techniques on a host-guest event of the supramolecular tetragonal prismatic nanocapsule $\mathbf{1}^{8+}$ which is capable of entrapping C_{60} and C_{70} fullerenes very effectively ($K_a > 10^7$ M^{-1}) (Scheme 1).[46-48] By using EXSY NMR and MD/aMD techniques a new and precise molecular perspective of the dynamics of the fullerene encapsulation inside the nanocapsule is obtained. The approach allows for the covering of multiple events, from the initial binding steps (at the ns-µs scale), to the competitive guest binding and exchange (up to the millisecond-second timescale) (see Scheme 1). This study shows that the encapsulation does not require to dismantle and reform the nanocapsule, and provides a detailed description of the role of aromatic groups at the entrance gate to control encapsulation and unbinding events. Overall, the encapsulation pathway is completely reconstructed at the molecular level for a series of guests. It is concluded that the capsule displays dynamic and recognition features typical of biological systems that allow for selective encapsulation of fullerenes. Finally, the encapsulation of azafullerene $(C_{59}N)_2$ within the supramolecular coordination capsule $\mathbf{1}^{8+}$ has been studied as a strategy to tweak the recognition pathway by simultaneous interactions at the cavity and at the gate due to its dumbbell shape.[49]

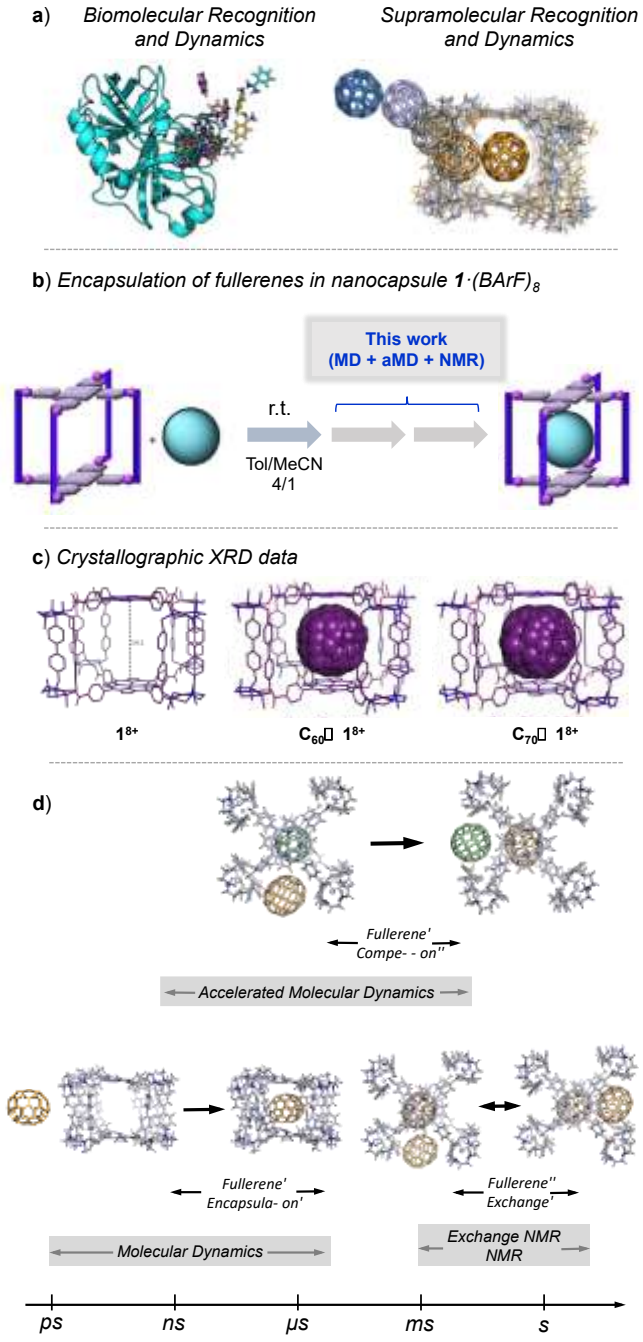

Scheme 1. a) Illustration of the similarities between biomolecular recognition and dynamics and supramolecular recognition and dynamics; b) Experimental encapsulation of C_{60} and C_{70} in nanocapsule $\mathbf{1}\cdot(BArF)_8$; c) crystal structure of $\mathbf{1}^{8+}$, $C_{60}\subset\mathbf{1}^{8+}$ and $C_{70}\subset\mathbf{1}^{8+}$; d) relevant processes, time scales, and techniques for the complete reconstruction of fullerene encapsulation, C_{70} (in light orange) and C_{60} (in green).

RESULTS

Nanocapsule $\mathbf{1}\cdot(BAr^F)_8$ consists of two opposing Zn-porphyrins linked by four bridging macrocyclic clips interconnected by four Pd^{II}-carboxylate bonds that define four entrance gates (Scheme 1 and Figure 1). $\mathbf{1}^{8+}$ has been reported as an efficient fullerene receptor for different sized fullerenes (from C_{60} to C_{84}). The release of the fullerene guest sequestered in

$\mathbf{1}^{8+}$ could be achieved by applying a solvent washing protocol,[46] or a redox-controlled guest exchange strategy,[50] highlighting the dynamic and reversible nature of the recognition process.

In order to explore in detail the dynamics of fullerene encapsulation, the in-out diffusion of C_{60} and C_{70} in $\mathbf{1}^{8+}$ under equilibrium conditions through ^{1}H-^{1}H exchange spectroscopy (EXSY) experiments was investigated.[51]

Dynamic NMR experiments. The experimental design required the coexistence of empty and filled capsule $\mathbf{1}^{8+}$, and for this reason sub-stoichiometric amounts of fullerenes were added to the capsule receptor. The exchange studies were conducted in a CD_3CN:[D_8]toluene 1:4 mixture to guarantee the proper solubility of both $\mathbf{1}^{8+}$ and the fullerene guests. A previous 1D and 2D-NMR characterization in CD_3CN has been described for $\mathbf{1}^{8+}$, $C_{60}\subset\mathbf{1}^{8+}$, and $C_{70}\subset\mathbf{1}^{8+}$ (Figures S1-S4).[46]

Fittingly, the ^{1}H-NMR analysis of the nanocapsule $\mathbf{1}^{8+}$ in the presence of sub-stoichiometric amounts of C_{60} (Figure 1) revealed two sets of signals for some of the aromatic protons, corresponding to empty $\mathbf{1}^{8+}$ and to the fullerene-containing capsule $C_{60}\subset\mathbf{1}^{8+}$ (protons b, h, j, k). A similar behaviour was observed when C_{70} was used as a guest (Figure S3).

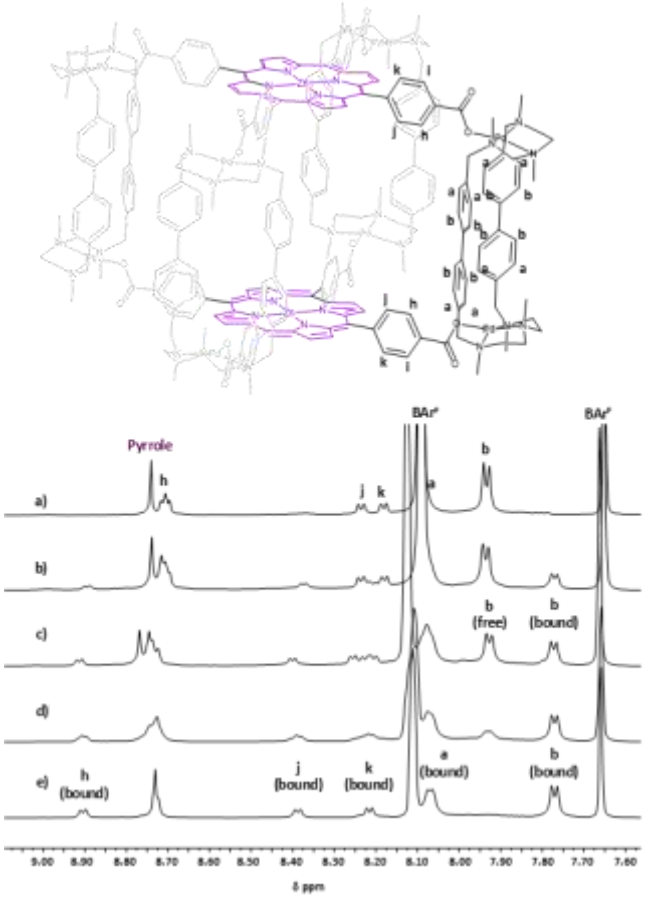

Figure 1. a) Expansion of ^{1}H NMR spectra (CH_3CN:[D_8]toluene 1:4, 600 MHz, 298 K) of the nanocapsule $\mathbf{1}^{8+}$ (0.52 mM) upon addition of (b) 0.33; (c) 0.46; (d) 0.66 and (e) 0.95 equivalents of C_{60}. Protons belonging to $C_{60}\subset\mathbf{1}^{8+}$ are labelled as "bound". Pyrrole protons appear in purple.

The 2D-NOESY NMR spectrum of a solution of $\mathbf{1}^{8+}$ in the presence of 0.33 equivalents of C_{60} displayed clear cross-peaks between signals of the host-guest complex $C_{60}\subset\mathbf{1}^{8+}$ and of the empty capsule $\mathbf{1}^{8+}$ (Figure 2). In fact, they were assigned as exchange cross-peaks since they were also detected in 2D-ROESY experiments, and they displayed the same sign as the diagonal peaks (Figure 2 and 3). Further ^{1}H-^{1}H 2D EXSY (NOESY) experiments using different sub-stoichiometric amounts of C_{60} (0.46 and 0.66 eq) and C_{70} (0.60 and 0.70 eq) led to analogous observations (see Figures S5-S6).

The rate constants for the exchange process ($k'_{on}= k_{on}$[G] and k_{off}) were calculated in the presence of various amounts of C_{60} and C_{70} (see details in SI and Schemes S1-S2). In particular, the intensities of the cross and diagonal peaks of the EXSY experiments measured with mixing times of 3 ms and 400 ms were employed (Table 1).[52-53] The obtained data allowed treating the encapsulation process as a pseudo-first order reaction since, under the investigated conditions, k'_{on} displayed a linear dependence on the concentration of C_{60} and C_{70}.[54-55] From these data, the corresponding exchange rates $k_{ex} = k'_{on} + k_{off}$ could be extracted (Table 1). On average, significantly larger association/dissociation events occurs per second for C_{60} than for C_{70}.

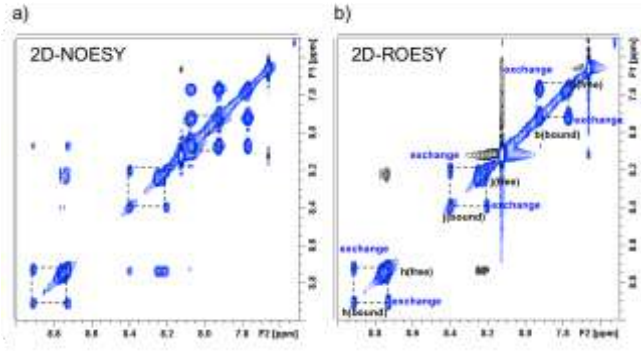

Figure 2. a) 2D-NOESY NMR spectrum (600 MHz, mixing time = 400 ms) of $\mathbf{1}^{8+}$ at 0.52 x 10^{-3} M CD_3CN / [D_8]toluene, at 298 K in the presence of 0.33 equivalents of C_{60}. Cross-peaks between protons signals at 7.93 and 7.77 ppm were used to determine the rate constant k'_{on} = 0.967 s^{-1} and k'_{off} = 2.286 s^{-1}. b) 2D-ROESY NMR spectrum (600 MHz, mixing time = 200 ms) of **1** at 0.52 x 10^{-3} M CD_3CN / [D_8]toluene, at 298 K in the presence of 0.33 equivalents of C_{60}.

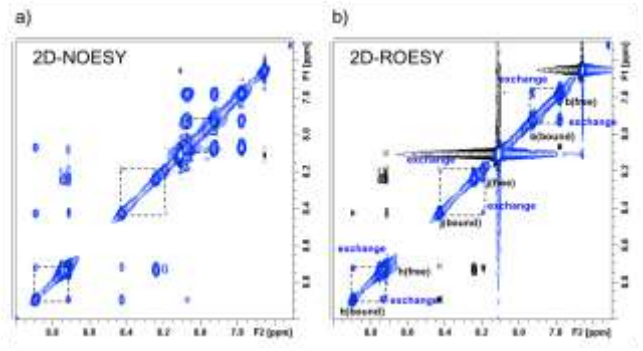

Figure 3. a) 2D-NOESY NMR spectrum (600 MHz, mixing time = 400 ms) of $\mathbf{1}^{8+}$ at 0.3·10^{-3} M CD_3CN:[D_8]toluene 1:4, at 298 K in the presence of 0.6 equivalents of C_{70}. Cross-peaks between protons signals at 7.93 and 7.78 ppm were used to determine the rate constant k'_{on} = 0.342 s^{-1} and k'_{off} = 0.236 s^{-1}. b) 2D-ROESY

NMR spectrum (600 MHz, mixing time = 200 ms) of $\mathbf{1}^{8+}$ at $0.3 \cdot 10^{-3}$ M CD_3CN:[D_8]toluene 1:4, at 298 K in the presence of 0.6 equivalents of C_{70}.

Table 1. Pseudo-first order rate constants for the guests (C_{60} and C_{70}) entry (k'_{on}) and departure (k_{off}) from the host $\mathbf{1}^{8+}$ determined by ^{1}H-^{1}H EXSY experiments. Second-order on-rate constants (k_{on}) were determined from the slope of the linear regression of k'_{on} vs [G] data. k_{on} values obtained from k_{off} and K_a ($k_{on} = K_a \cdot k_{off}$) were indicated in brackets.

Guest	Equiv.	k_{off} (s^{-1})	k'_{on} (s^{-1})	k_{ex} (s^{-1})	k_{on} ($M^{-1}s^{-1}$)
C_{60}	0.33	2.47±0.19	1,04±0.07	3.51±0.20	$(6.91±0.05)\cdot10^7$
	0.46	2.49±0.11	1,90±0.09	4.39±0.14	$(6.96±0.03)\cdot10^7$
	0.66	1.35±0.04	2.61±0.15	3.95±0.15	$(3.77±0.01)\cdot10^7$
				average:	$4\cdot10^7$ ($5.9\cdot10^7$)
C_{70}	0.6	0.22±0.03	0.53±0.08	0.75±0.08	$(8.76±1.04)\cdot10^7$
	0.7	0.28±0.03	0.75±0.08	0.98±0.09	$(1.11±0.14)\cdot10^8$
				average:	$1\cdot10^8$ ($9.9\cdot10^7$)

Although some statistical dispersion was detected in determining the dissociation rate constants of C_{60}, the obtained k_{off} were significantly (ca. one order of magnitude) faster than that measured for C_{70}, indicating a higher affinity for the encapsulation of C_{70}. These results are in good agreement with the binding constant previously calculated from UV-vis and fluorescence titration experiments (K_a= 2.8 x 10^7 M^{-1} for C_{60} and K_a= 3.98 x 10^8 M^{-1} for C_{70}).[46] Finally, the second-order association rate constants k_{on} ($k_{on} = K_a$ x k_{off}) for C_{60} and C_{70} were determined from the slope of the curve k'_{on} vs. guest concentration (see Supporting Info) and from the direct relationship of k_{on} with k_{off} (extracted from the EXSY experiments) and the K_a constants (obtained from fluorescence titration experiments).[46] On average, k_{on} values of $4.9\cdot10^7$ $M^{-1}s^{-1}$ and $9.9\cdot10^7$ $M^{-1}s^{-1}$ were calculated for C_{60} and C_{70}, respectively.

Therefore, the ^{1}H-^{1}H exchange spectroscopy (EXSY-NMR) experiments indicate that *i*) guest exchange occurs in the range of hundreds of milliseconds to seconds for both C_{60} and C_{70} and that *ii*) the higher affinity of $\mathbf{1}^{8+}$ toward the encapsulation of C_{70} arises from a slower dissociation of $C_{70}\subset\mathbf{1}^{8+}$ compared to $C_{60}\subset\mathbf{1}^{8+}$, strongly suggesting the existence of stronger interactions for the $C_{70}\subset\mathbf{1}^{8+}$ complex. Hence, a mechanistic explanation of these results at the molecular level is required. In this context, we reasoned that the development of a novel methodology for the full understanding of these dynamic recognition events at the first stages of the interaction would be of high interest to determine the structural parameters and molecular recognition forces that govern the observed selectivity.

Molecular Dynamics (MD) of fullerene encapsulation. To unravel the essential details of fullerene encapsulation and selectivity, the encapsulation of one molecule of C_{70} in $\mathbf{1}^{8+}$ was studied by long-time scale MD simulations. An analogous analysis was performed for C_{60}. Then, aMD technique was applied for a competitive encapsulation experiment with one molecule of C_{60} and one of C_{70}. Finally, the intricate encapsulation of $(C_{59}N)_2$ is explored.

Supramolecular capsule flexibility/adaptablity. First, the guest-free nanocapsule $\mathbf{1}\cdot(Cl)_8$ was subjected to MD simulations (three replicas of 2.5 μs, see SI for computational details). Far from the rigid view of the X-ray structure, the supramolecular capsule showed exceptional flexibility in solution.[46] Twists of the four capsule clips that define the four entrance gates provide great flexibility to the system (see Video S1). This is translated to ZnPorph···ZnPorph distances ranging from 11.3 to 15.8 Å being the average distance 13.6 ± 0.5 Å in solution, close to the 14.1 Å found in the XRD structure (see Figure S7). These results highlight the intrinsic flexibility of the supramolecular capsule that its key to explain its affinity for fullerenes of different size (from C_{60} to C_{84}). Therefore, the $\mathbf{1}^{8+}$ in the guest-free form samples a large number of thermally accessible conformations other than the one represented in the X-ray structure. This ability is reminiscent of proteins as well of the flexibility reported in some MOFs.[56-57] The inner flexibility of $\mathbf{1}^{8+}$ evokes to the concept of conformational selection used to elucidate molecular recognition processes in biomolecules, which is based on the pre-existence of all conformations in solution.[4] Then, the ligand selects and stabilizes the conformations displaying proper binding features that causes a shift on the relative populations of the conformational ensemble. The question is whether fullerene encapsulation is going to display similar features as biomolecular recognition processes and alter the relative populations of conformational states sampled by the guest-free capsule.

General features of C_{70} encapsulation process. To elucidate the essential details of the recognition process at the molecular level, MD simulations in the presence of fullerenes in solution were performed. The encapsulation process in equimolar amounts of C_{70} and capsule $\mathbf{1}\cdot Cl_8$ was simulated in multiple replicas to obtain a statistical characterization of the binding event (30 replicas in total accumulating 75 μs of simulation time, see Figure 4 and Figures S8-11)**.** The fullerene was placed in an arbitrary position 25 Å away from the center of mass of the supramolecular capsule and was allowed spontaneously diffusing along the MD trajectories (see Figure 4a and 4c). The distance between the center of masses of C_{70} and the supramolecular capsule, d($\mathbf{1}^{COM}$-C_{70}^{COM}) was monitored along the MD simulation to capture the encapsulation event (distances below 2 Å indicate C_{70} encapsulation at the center of the capsule). Complete encapsulation was observed in twenty-six out of thirty replicas of 2.5 μs MD simulations (86% of binding events) indicating that fullerene recognition and binding takes place in the nanosecond-microsecond time scale. The visual inspection of MD simulations revealed the following features (see Videos S2 and S3). In all cases, C_{70} was observed to firstly interact with one of the four entrance gates of the capsule, being transiently stabilized in this position. The permanence in the gate ranged from 5 ns to few microseconds revealing the existence of metastable intermediate states and multiple binding pathways prior complete encapsulation that were not identified previously from XRD structures and NMR experiments (see Figures 4a and 4b). After subtle but significant nanocapsule rearrangements described below, the fullerene subsequently enters to the center of the cavity sitting in between the two porphyrin units (an axis can be drawn from one Zn center to the other, passing through the center of C_{70} sphere). The MD predicted bound complex coincides with XRD and DFT structures.[46] Despite this fixation, the fullerene present ability to rotate inside the cavity. The latter, together with the transient state observed prior the complete entrance of

C_{70}, suggested a barrier for a) recognizing the gate, b) entering through the gate and c) being fixed while rotating at the center of the cavity.

To offer a complete picture of the metastable states and dynamical steps of the recognition and binding process, the free energy landscape (FEL) of the encapsulation was reconstructed from an accumulated simulation time of 75 μs (see Figure 4b). The FEL was represented by two coordinates: the distance between the center of masses (COM) of C_{70} and the supramolecular capsule, d($\mathbf{1}^{COM}$-C_{70}^{COM}), and the ZnPorph···ZnPorph distances**.** The FEL obtained from these two coordinates revealed five metastable states: Unbound (**U**, d($\mathbf{1}^{COM}$-C_{70}^{COM}) > 20 Å, Recognition (**R**, d($\mathbf{1}^{COM}$-C_{70}^{COM}) ~13 Å), Intermediate 1 ($\mathbf{I_1}$, d($\mathbf{1}^{COM}$-C_{70}^{COM}) ~10 Å), Intermediate 2 ($\mathbf{I_2}$, d($\mathbf{1}^{COM}$-C_{70}^{COM}) ~7 Å), and Bound (**B,** d(C_{70}^{COM}-1^{COM}) < 2 Å) states. Fullerene recognition (from solvent to the gate) takes place in few nanoseconds with a small barrier of approximately 1 kcal/mol associated to the transition from **U** to **R**. Then, the fullerene molecule is rapidly stabilized at the center of the gate ($\mathbf{I_2}$) and eventually overcomes a barrier of roughly 4 kcal/mol to target the center of the supramolecular capsule (**B**). The latter process takes place in the nanosecond-microsecond time scale indicating the fast recognition and binding of C_{70} by the supramolecular capsule. The $\mathbf{I_2}$**-B** transition involves, first, a transient expansion of the ZnPorph···ZnPorph distance from 14 to 15 Å to let the fullerene target the center of the capsule and, second, a compression of the capsule towards 13 Å to stabilize the fullerene molecule. As shown in the FEL of Figure 4b, in the bound state, the ZnPorph···ZnPorph distance of the minima is shorter (13 Å) than in other states (above 13.5 Å as in the guest-free capsule). Therefore, C_{70} binding (**B**) alters the dynamics of the capsule inducing a population shift towards shorter ZnPorph···ZnPorph distances, restricting the flexibility of the nanocapsule by increasing the interactions between the fullerene and the ZnPorph moieties**.** C_{70} selects and stabilizes scarcely populated conformations in the guest-free capsule (ZnPorph···ZnPorph distances below 13 Å) shifting the conformational ensemble towards a more compressed nanocapsule (see Figure S9).

Moreover, interconversion between two intermediate states, $\mathbf{I_2}$ and $\mathbf{I_1}$, was frequently observed at the entrance gate. In state $\mathbf{I_2}$, the fullerene lays in the center of the gate, featuring a larger ZnPorph···ZnPorph distance (14.0 Å average) and stabilized by the 'hand-glove-effect' exerted by the π-π interactions of the fullerene with the phenyl moieties of the clips. On the other hand, in state $\mathbf{I_1}$ the fullerene is stacked in the bottom of the entrance gate stabilized by two phenyl rings connecting the porphyrin moiety and carboxylate groups directly bound to the palladium atoms. Unbinding of C_{70} from the bound state **B** is not observed in the microsecond time scale simulations. This is consistent with NMR experiments indicating that guest unbinding and exchange event occurs in the millisecond to second time-scale.

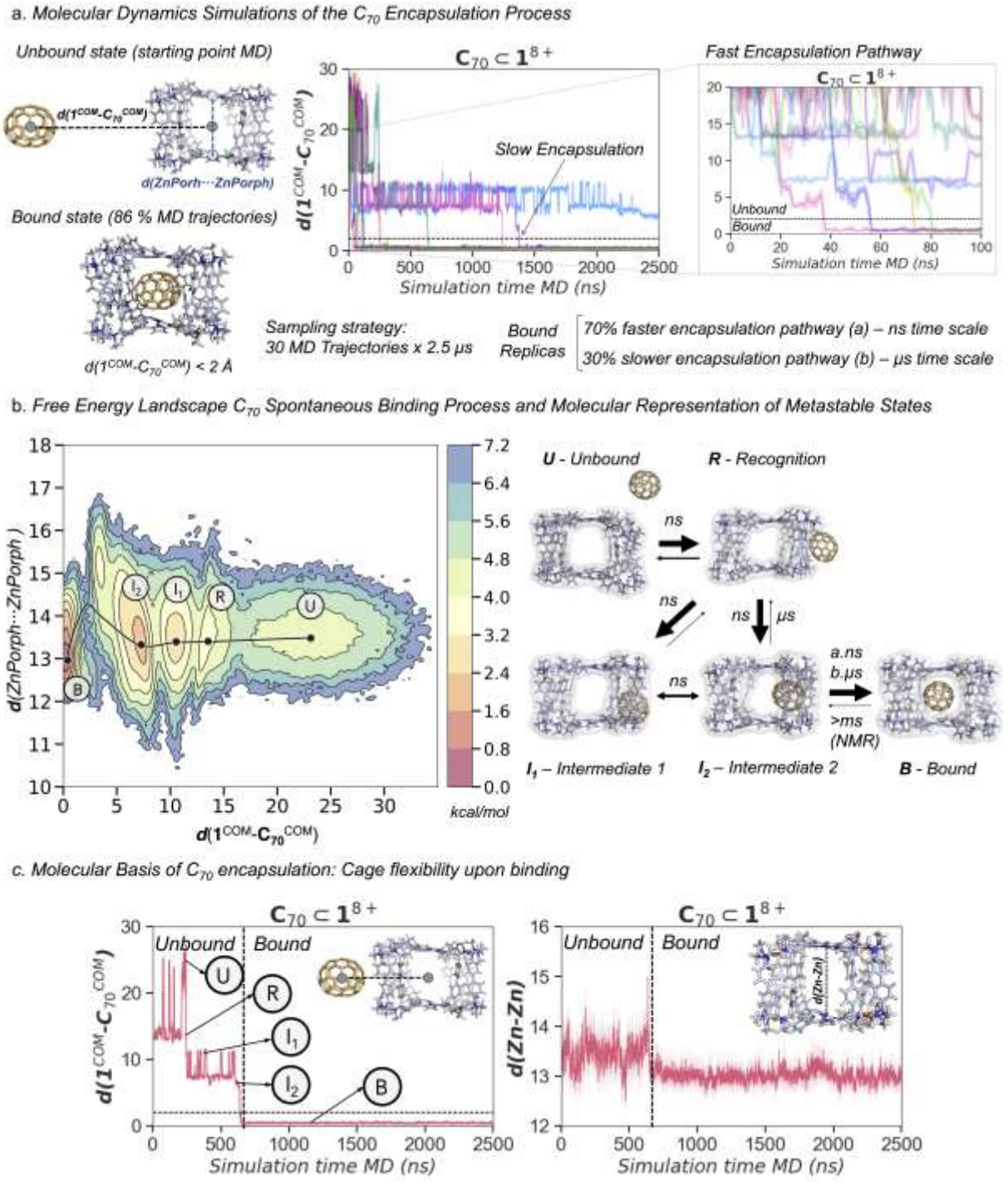

Figure 4. a) Plot of the distance between the center of masses of C_{70} and the supramolecular capsule, d(C_{70}^{COM}-**1**^{COM}) for ten representative 2.5 μs replicas of MD simulations. Distances below 2 Å indicate complete C_{70} encapsulation (dashed horizontal line). Spontaneous binding is observed in nine out of ten of the selected replicas. Inset plot of the first 100 ns where four replicas display fullerene encapsulation in the tenths of nanoseconds time-scale (fast encapsulation). b) Reconstructed Free Energy Landscape (FEL) of the spontaneous encapsulation process of C_{70} obtained from an accumulated simulation time of 75 μs of MD simulations. The FEL has been reconstructed using d(**1**^{COM}-C_{70}^{COM}) and ZnPorph···ZnPorph distances. Fives relevant metastable states are identified: Unbound (**U**), Recognition (**R**), Intermediate 1 (**I**$_1$), Intermediate 2 (**I**$_2$), and Bound (**B**) states. Molecular representation of each state. The width of the arrow indicates the most frequent events observed and the time scales implied from MD simulations and NMR experiments. c) Plot of the distance (in Å) between the center of masses of C_{70} and the supramolecular capsule, d(**1**^{COM}-C_{70}^{COM}) along 2.5 μs of a representative replica of MD simulation. Distances below 2 Å indicate complete C_{70} encapsulation (dashed horizontal line). Plot of the distance (in Å) between ZnPorph···ZnPorph along 2.5 μs of a representative replica of MD simulation. Vertical dashed line indicates the moment that full encapsulation takes place.

Molecular basis of C_{70} dynamic encapsulation process at ns-µs timescale. To gain deeper insight into the chemical nature of encapsulation barrier (transition from **I_2** to **B**), a detailed study of the molecular basis of possible fullerene recognition pathways was performed based on monitoring key distances between different parts of the cavity as well as analyzing the dimensions of the entrance gate (see Figures 4c and 5). The MD simulations revealed that the orientation of the phenyl rings connecting the porphyrin moiety and carboxylate groups directly bound to the palladium atoms is key to allow the entrance of the fullerene (Figure 5). In each of the four entrances there are four phenyl rings that act as a gate for fullerene binding. MD simulations unveiled that the entrance gate could be found in four major conformations: open, partially open, lateral displacement, and closed (see Figure 5a). If the distance between Ar-H···H-Ar pairs at the top and at the bottom of the gate are both higher than 9 Å then the gate is found in an open conformation, displaying an entrance gate of 80-90 $Å^2$ (Figure 5b). However, if this distance falls to 7 Å because phenyl rings reorient (one phenyl pointing towards the gate and one phenyl pointing away from the gate) or 5 Å (both phenyls pointing towards the gate) the size of the entrance gate is progressively squeezed, decreasing the entrance gate area down to 50 $Å^2$ for the completely closed case (see Figure 5b). MD simulations show that the entrance gate area fluctuates along time, displaying open-closed transitions in the nanosecond to microsecond time scale that are key for C_{70} binding and stabilization (Figure 5c). Based on the MD simulations, encapsulation of C_{70} is not possible in the completely closed conformation (0% of binding events). Encapsulation is only taking place when entrance gate areas above 65 $Å^2$ are sampled (partially open, see Figures S10-S11 and Table S3). Interestingly the fullerene is rapidly captured by the capsule if the Ar-H of the phenyl rings are found in an open conformation, i.e. not pointing towards the fullerene (see different conformations in Figure 5a). When all phenyls are in a closed conformation, the fullerene is stabilized in the gate of the capsule (**I_1** and **I_2**) until some phenyl rings rotate to trigger the full entrance or the fullerene returns to the solvent to target another gate (see plot in Figure 5c). Therefore, two binding pathways coexist, one fast and one slow, determined by the conformations of the entrance gate. Thereby, if the fullerene recognizes an entrance of the capsule with all phenyls in the open conformation the binding process occurs in the nanosecond time scale (less than 100 ns, 70% of binding events, see Figure 5a, S10, and S11 and Video S2) whereas if some of the phenyls are in the closed conformation the binding process is significantly slowed down to the microsecond time scale (see Figure 5c, S10, and S11 and Video S3). Therefore, the orientation and rate of rotation of the phenyl rings becomes the rate-limiting step of the recognition process (4 kcal/mol barrier from **I_2** to **B** in Figure 4b). The Ar-H···H-Ar distances between the porphyrinic phenyl moieties show the subtle but significant barrier that these multiple aromatic C-H bonds cause to the squeezing of C_{70} inside the cavity, and furthermore, they stabilize the C_{70} right at the center of the cavity once it has entered, by preventing the displacement of the fullerene in any direction. The number of open-closed transitions of all nanocapsule gates is significantly restrained upon fullerene encapsulation showing a tendency towards fixing entrance gate areas around 70 $Å^2$ (Figure 5c). This stabilizing effect can be key to hinder the unbinding process, which takes place at much longer time scales (ms-s) based on NMR experiments. $\mathbf{1}^{8+}$ has the ability of activating and deactivating its intrinsic flexibility to favor binding and retain the guest, respectively. Therefore, the guest encapsulation process is tightly coupled to the intrinsic dynamics of $\mathbf{1}^{8+}$.

Besides the role of the phenyl moieties, also the "hand-glove" effect from the biphenyl linkers of the clips that decorate the entrance gate help in understanding the transient intermediate formation (**I_1** and **I_2**), by stabilizing the C_{70} molecule through C-H…π interactions and being responsible of pushing the C_{70} inside the cavity when going from **I_2** to **B**. Upon full encapsulation (Figure 4c), the ZnPorph···ZnPorph distance is reduced from an average distance of 13.6 ± 0.5 Å down to 13.0 ± 0.3 Å significantly restricting the flexibility of the nanocapsule (see Figure 4a and 4c) but C_{70} keeps rotating inside the cavity. Although rotation in all directions is observed, the binding with the supramolecular capsule retains C_{70} horizontally-oriented most of the time whereas infrequently samples C_{70} in the vertical orientation (see Figure S12). Therefore, the nanocapsule is able to impose a certain orientation to the fullerenes in order to maximize the π-interaction with the porphyrin and to generate a more stable complex. DFT calculations and the analysis of interactions in the bound complex have been performed before and showed that the preferred orientation matches with the predicted in the MD simulations.[46] These observations show significant parallelisms with conformational selection mechanisms in biomolecular recognition, where binding readily occurs when $\mathbf{1}^{8+}$ displays the proper conformation. However, in a number of simulations the ligand is inducing the conformational changes required to complete the **I_2** to **B** transition, in particular, when C_{70} finds the entrance gate not fully open. In all cases, a population shift towards a more rigid nanocapsule that stabilizes the bound state and slows down unbinding is observed upon complete encapsulation. As enzymes with substrates or inhibitors, the nanocapsule is displaying open-closed transitions that are key for guest recognition, binding, and unbinding.[58]

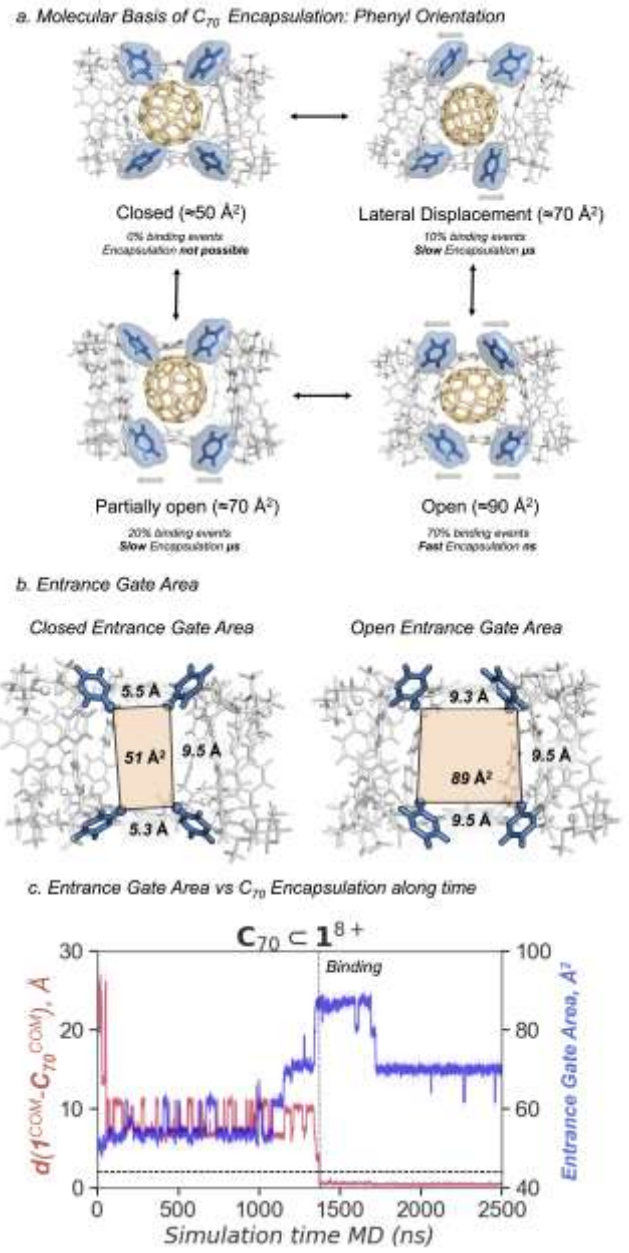

Figure 5. a) Different conformations displayed by each gate of the supramolecular capsule defined by the orientation of the phenyl rings connecting the porphyrin moiety and carboxylate groups directly bound to the palladium atoms. Arrows indicate rotations of phenyl groups with respect to the closed conformation. The approximated entrance gate are is specified in parenthesis. The percentage of binding events among the 30 replicas of MD simulations is also represented. b) Entrance gate area (in $Å^2$) is approximated as a trapezium defined by the top and bottom Ar-H···H-Ar distances calculated between the porphyrinic phenyl moieties and an average gate height of 9.5 Å. Typical Ar-H···H-Ar distances are 9-10 Å (open), 7-8 Å (one phenyl open and one phenyl closed), 5-6 Å (closed). Representative distances and entrance gate areas for a fully closed and fully open entrance gate are also depicted. c) Plot of the distance (red line) between the center of masses of C_{70} and the supramolecular capsule, $d(\mathbf{1}^{COM}\text{-}C_{70}{}^{COM})$, and entrance gate area (blue line) along a representative 2.5 µs replica of MD simulations. Complete encapsulation ($d(\mathbf{1}^{COM}\text{-}C_{70}{}^{COM})$ below 2 Å) takes place when the entrance gate area significantly increases.

General Features of C_{60} Encapsulation Process. Then, the encapsulation process of C_{60} within capsule $\mathbf{1}\cdot Cl_8$ was investigated. The FEL of C_{60} was reconstructed from 30 replicas of 2.5 µs of MD simulations as described for C_{70}. Likewise to the encapsulation of C_{70}, C_{60} is also forming the same transient intermediates featuring the interaction with one of the four entrance gates of the capsules, being stabilized by the 'hand-glove-effect' of the biphenyl units exposed to the gate and stopped from entering by the slight blocking effect exerted by the porphyrinic phenyl moieties (see FEL in Figure S13). Once the phenyl rings reorient, the C_{60} molecule overrides the slight barrier and it is stabilized at the center of the cavity, analogously to C_{70}. The transition from $\mathbf{I_2}$ to **B** states is in the same order of magnitude than the one observed for C_{70} remaining in the nanosecond to microsecond time scale. In comparison with C_{70}, the transition between $\mathbf{I_2}$ to **B** for C_{60} requires a smaller expansion of the nanocapsule (ZnPorph···ZnPorph distance lower than 14 Å) but the nanocapsule is more compressed upon binding (average ZnPorph···ZnPorph of 12.7 ± 0.3 Å for C_{60} and 13.0 ± 0.3 Å for C_{70}), which is in line with the smaller size of C_{60}. Finally, the molecular basis of the encapsulation process follows similar general features of C_{70} (see Figure S14). In general, C_{60} shows higher mobility inside the capsule indicating weaker non-covalent interactions than in C_{70}. The encapsulation of C_{60} required extra compression of the nanocapsule prompting frequent transient extensions of ZnPorph···ZnPorph. These transient events can facilitate unbinding. This is consistent with the faster k_{off} determined for C_{60} by EXSY experiments in comparison with C_{70}. However, the higher affinity toward the encapsulation of C_{70} over C_{60} cannot be completely explained from single fullerene binding MD simulations. To this end, competition experiments are required to understand the origins of nanocapsule selectivity.

Computational nanoreactor: C_{60} versus C_{70} competition and guest exchange mechanism with aMD. Based on EXSY-NMR results, the guest exchange and competition takes place in slower time-scales (ms-s) than the encapsulation

process (ns-μs). To access time-scales relevant for sampling rare events (ms-s) in supramolecular systems, we resorted to accelerated molecular dynamics (aMD) simulations (see SI for details). In general, hundreds of nanosecond aMD simulations are able to capture millisecond timescale events as applied in both globular and membrane proteins.[59] The advantage of aMD over other enhanced sampling techniques is that the sampling is completely unconstrained, therefore, unguided spontaneous binding/exchange among multiple guests can be studied without the need of specifying any reaction coordinate. Here, the aim was to use a combination of MD and aMD as a tool to mimic computational nanoreactors to access millisecond time scales events occurring in the competition experiment for the encapsulation of C_{60} versus C_{70} in $\mathbf{1}^{8+}$. To this end, five replicas of 8 μs of combined MD+aMD simulations were used to study the molecular basis of guest competition and exchange in the presence of C_{60} and C_{70}. The simulations start with conventional MD and aMD simulations are activated once the first fullerene targets the center of the capsule. By performing MD+aMD experiments under the same conditions as described above but including one molecule of C_{60} and one molecule of C_{70}, we are able to observe (5-replicate average) the real-time competition between the two guests (see Video S4). We monitored the distances between the center of masses of C_{70} and C_{60} and the supramolecular capsule, d($\mathbf{1}^{COM}$-C_{70}^{COM}) and d($\mathbf{1}^{COM}$-C_{60}^{COM}) along the MD simulation to study the competition event. Among five replicas of MD+aMD, both C_{60} and C_{70} can sample the gates of the nanocapsule and encapsulation of either C_{60} or C_{70} can be observed depending on the orientation of phenyl rings. In general, competition of fullerenes slows down the encapsulation process towards microsecond time scales. If C_{70} is the first to target the center of the nanocapsule, it remains there for the rest of the simulation and no replacement by C_{60} is observed (see Figure S15). However, if C_{60} is the one that eventually targets first the center of the cavity, then guest exchange is observed. As shown in Figure 6, C_{60} binding takes place after 5 μs of MD simulation time. After 500 ns of aMD (actual millisecond timescale), C_{70} pushes C_{60}, which is expelled from the cavity back to the gate and is C_{70} the one that is fully encapsulated and remains there for the rest of the simulation (see Video S4). In a closer look at the precise event of full encapsulation of C_{70}, it turns out that it is occurring when the phenyl moieties are in the 'open' disposition, as shown in Figure 5.

The facile encapsulation for C_{60} compared to C_{70}, and the even more facile release of C_{60} compared to C_{70} under the non-equilibrium regime of MD point towards a similar trend than the observations by EXSY-NMR experiments. The determined k_{off} values are one order of magnitude slower for C_{70} than for C_{60}, while k'_{on} is also much faster for C_{60} than for C_{70}. Therefore, C_{60} performs in and out movements at faster rates than C_{70}. Moreover, C_{70} is the one that remains in the nanocapsule under thermodynamic equilibrium conditions (millisecond to second time scale, $K_a(C_{70}) \sim 10 \times K_a(C_{60})$). Thus, the combination of MD and aMD simulations can be used as a computational tool that mimic a nanoreactor to predict the preference among multiple guests. This protocol can be generalized to predict the preference for other guests and, then, coupled to exchange NMR experiments to obtain on and off rates to completely reconstruct encapsulation processes. Moreover, the gathered information on the binding and exchange pathways can be used to identify robust reaction coordinates to guide constrained enhanced sampling simulations.[11]

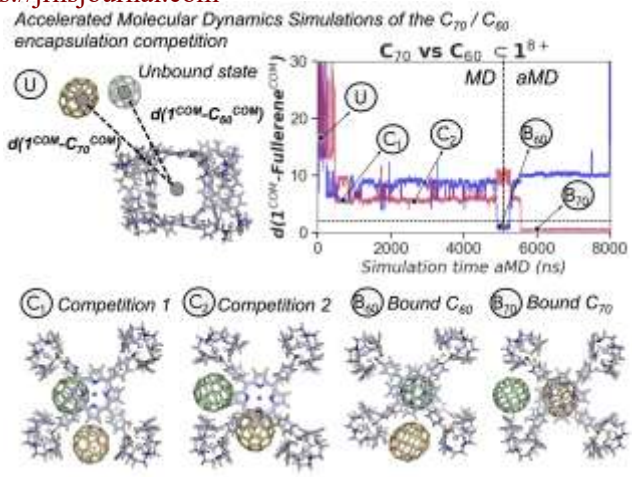

Figure 6. Plot of the distance between the center of mass of C_{70} and C_{60} and the supramolecular capsule, d(C_{70}^{COM}-$\mathbf{1}^{COM}$) in red and d(C_{60}^{COM}-$\mathbf{1}^{COM}$) in blue respectively for a representative 8 μs replica of accelerated molecular dynamic simulations. Distances below 2 Å indicate complete fullerene encapsulation (dashed horizontal line). Molecular representation of five relevant states sampled along the competition and exchange process of C_{70} (orange) and C_{60} (green): the Unbound (**U**, both C_{70} and C_{60} are not interacting with the capsule), Competition 1 (**C_1**, C_{60} closer to the cavity than C_{70}), Competition 2 (**C_2**, C_{70} closer to the cavity than C_{60}), Bound C_{60} (**B_{60}**), and Bound C_{70} (**B_{70}**) states.

Encapsulation of dumbbell-shaped azafullerene ($C_{59}N)_2$: tweaking recognition pathways and affinity. The plasticity of $\mathbf{1}^{8+}$ is key to selectively encapsulate a wide range of fullerenes from C_{60} to C_{84} with high association constants, $K_a > 10^7$ M^{-1}. Fullerenes above this size cannot fit and pass through the gates of $\mathbf{1}^{8+}$ while below this number of carbons cannot be stabilized. The question is whether the association recognition pathway can also be determinant to control selectivity. To answer this question and assess the predictive power of the computational protocol, we explored the recognition pathways of a dumbbell-shaped fullerene, azafullerene, $(C_{59}N)_2$, a model guest to tune the recognition pathway by kinetically trapping an intermediate state and slowing down the recognition process. This system represents a perfect candidate for simultaneously altering the recognition pathway and affinity because, in terms of size, each individual $C_{59}N$ spherical moiety can fit inside $\mathbf{1}^{8+}$ but the extra monomer can compromise both the recognition process and the stability of the bound complex. The encapsulation of $(C_{59}N)_2$ in a supramolecular coordination capsule has not been explored before and the nature of the potential bound complex is unknown. Supramolecular recognition of $(C_{59}N)_2$ has only been reported within carbon nanotubes (CNT)[60] and cycloparaphenylene (CPP) rings.[61-62]

To explore the essential molecular details of the recognition process of $(C_{59}N)_2$, a similar protocol as described above for C_{70} was used. A total of ten replicas of 5 μs and ten of 2.5 μs of MD simulations were performed to study the spontaneous encapsulation of azafullerene. The complete encapsulation, $(C_{59}N)_2 \subset \mathbf{1}^{8+}$, was observed in two out of twenty replicas (10% of binding events in 75 μs of accumulated simulation time) indicating that azafullerene recognition is possible but is significantly slowed down compared to C_{70} and C_{60}. In average,

the binding process is not occurring at the nanosecond-microsecond time scale. A visual inspection of the spontaneous binding MD trajectories revealed that $(C_{59}N)_2$ remains trapped in metastable intermediate states in most of the simulations, even though some replicas are extended up to 5 μs, suggesting a higher barrier for entering through the gate (link a video S5 and S6). To explore the precise dynamical steps and conformations of the recognition process, the FEL of $(C_{59}N)_2$ encapsulation was reconstructed from an accumulated simulation time of 75 μs. To obtain a comparable FEL as in C_{70} and C_{60}, three center of masses (COM) of $(C_{59}N)_2$ were monitored (the COM of each $C_{59}N$ unit and the global COM, Figure 7a) and, then, for each frame the COM displaying the minimum distance with the COM of $\mathbf{1}^{8+}$ is collected for the analysis (see Figure 7a). As shown in Figure 7b and 7c, the FEL also displays similar metastable states as C_{70} and C_{60}, but featuring a significant redistribution of relative populations. The intermediate $\mathbf{I_1}$ is now the most stable state being significantly stabilized in comparison to single fullerenes. The recognition state (**R**) is also more populated. On the contrary, the intermediate state $\mathbf{I_2}$, which is the connection with the bound (**B**) state, is significantly less visited lowering the chances of targeting the center of $\mathbf{1}^{8+}$ in the microsecond time-scale. In this limited simulation time totalling 75 μs, the **B** state is scarcely populated in comparison to C_{70} and C_{60}. Therefore, in $(C_{59}N)_2$ there is a redistribution of populations with respect to C_{70} and C_{60} favouring early stage encapsulation $\mathbf{I_1}$ and **R** states.

Careful analysis of representative structures of each state revealed that the intermediate state $\mathbf{I_1}$ exist as an ensemble of different conformations. In total, three orientations of $(C_{59}N)_2$ with respect to $\mathbf{1}^{8+}$ coexist in solution in the $\mathbf{I_1}$ basin ($\mathbf{I_1}$, $\mathbf{I_1}$', and $\mathbf{I_1}$", see Figure 7c). In $\mathbf{I_1}$', $(C_{59}N)_2$ is oriented in parallel to the ZnPorph···ZnPorph axis and each $C_{59}N$ unit is stabilized by two phenyl rings at the bottom and at the top of the entrance gate and also by the "hand-glove" effect from the biphenyl linkers of the clips. In the case of $\mathbf{I_1}$", $(C_{59}N)_2$ also adopts a parallel orientation but both $(C_{59}N)_2$ fullerene units staple the bottom of the entrance gate from the solvent and gate sites. Both $\mathbf{I_1}$' and $\mathbf{I_1}$" became remarkably stable in the simulations maximizing the interactions between $\mathbf{1}^{8+}$ and $(C_{59}N)_2$ and kinetically trapping the azafullerene in unproductive states for the encapsulation process. Moreover, a collateral effect is that in both $\mathbf{I_1}$' and $\mathbf{I_1}$" the phenyl rings rapidly reorient to stabilize $(C_{59}N)_2$ through CH…π interactions. This rotation induces the closure of the entrance gate decreasing the options of encapsulation through this gate. The transition from $\mathbf{I_1}$' and $\mathbf{I_1}$" to $\mathbf{I_2}$ is rarely observed and when it occurs the entrance gate is closed. Therefore, $(C_{59}N)_2$ needs to be expelled back to solvent and target another gate with less steric hindrance. Therefore, populating these intermediate states introduces complexity to the binding pathway and significantly slows down the full encapsulation process. In addition, the intermediate $\mathbf{I_2}$, with one $C_{59}N$ moiety located at the center of the entrance gate, is poorly stable because the other $C_{59}N$ unit cannot establish strong interactions with the capsule reducing its stability. In the two binding events observed, $(C_{59}N)_2$ went directly from the solvent to $\mathbf{I_2}$, where it stayed for few hundreds of nanoseconds after targeting the center of $\mathbf{1}^{8+}$. The bound state **B** is characterized by one $C_{59}N$ moiety sitting in the center of the capsule between the two ZnPorph while the other is stabilized at the entrance of the gate. Once one $C_{59}N$ is captured, the ZnPorph···ZnPorph distance is reduced to 13.0 ± 0.4 Å, similar to C_{60} and showing higher fluctuations than C_{70}. Interestingly, the slow binding left enough time to phenyl moieties to readjust to stabilize the azafullerene in $\mathbf{I_2}$ complicating the full encapsulation. In both cases, the encapsulation takes place in a partially open entrance gate. Therefore, the dumbbell fullerene induces and stabilizes the entrance gate closure. Moreover, an alternative state, $\mathbf{I_2}$', is transiently populated with each $C_{59}N$ unit sitting in contiguous entrance gates (see Figure 7c). To sum up, the pathway that followed $(C_{59}N)_2$ to target the center of the supramolecular capsule (**B**) became more complex involving a higher number of intermediate states and overcoming higher energy barriers than in C_{70} and C_{60}. The fullerene perfectly fits inside $\mathbf{1}^{8+}$ but in the encapsulation process is kinetically trapped in an intermediate state significantly slowing down binding and recognition.

Finally, the stability of $(C_{59}N)_2$, C_{70}, and C_{60} inside $\mathbf{1}^{8+}$ is evaluated by monitoring how the distance between the center of masses of the supramolecular capsule and the fullerene fluctuates upon binding (see Figure 7d). Interestingly, C_{60} is more mobile (0.55 ± 0.5 Å) inside $\mathbf{1}^{8+}$ than C_{70} (0.41 ± 0.2 Å) in line with the reported K_a and NMR studies that pointed out a higher resistance towards dissociation for the latter under thermodynamic equilibrium conditions. Interestingly, a wider distribution and a displacement towards longer distances (0.89 ± 0.6 Å) is observed for $(C_{59}N)_2$. These results show that $(C_{59}N)_2$ is less stable in the center of $\mathbf{1}^{8+}$ increasing the opportunities to escape from the capsule. To corroborate the computational predictions, the association constant of $(C_{59}N)_2$ into $\mathbf{1}^{8+}$ was measured, $K_a = 9.4(\pm0.5)\cdot10^5\ M^{-1}$ (see Figure S17). This value is one and two order of magnitudes lower than the K_a reported for C_{60} (30-fold lower) and C_{70} (420-fold lower), respectively. Further modifications in $\mathbf{1}^{8+}$ will be required to capture $(C_{59}N)_2$ with high affinity. Tuning recognition pathways and the plasticity and dynamics of the host offers new routes towards predicting affinities and improving rational design of supramolecular recognition platforms. Research in this direction is underway in our laboratories. This strategy has allowed assessing the dynamic limits of the capsule in terms of recognition pathway.

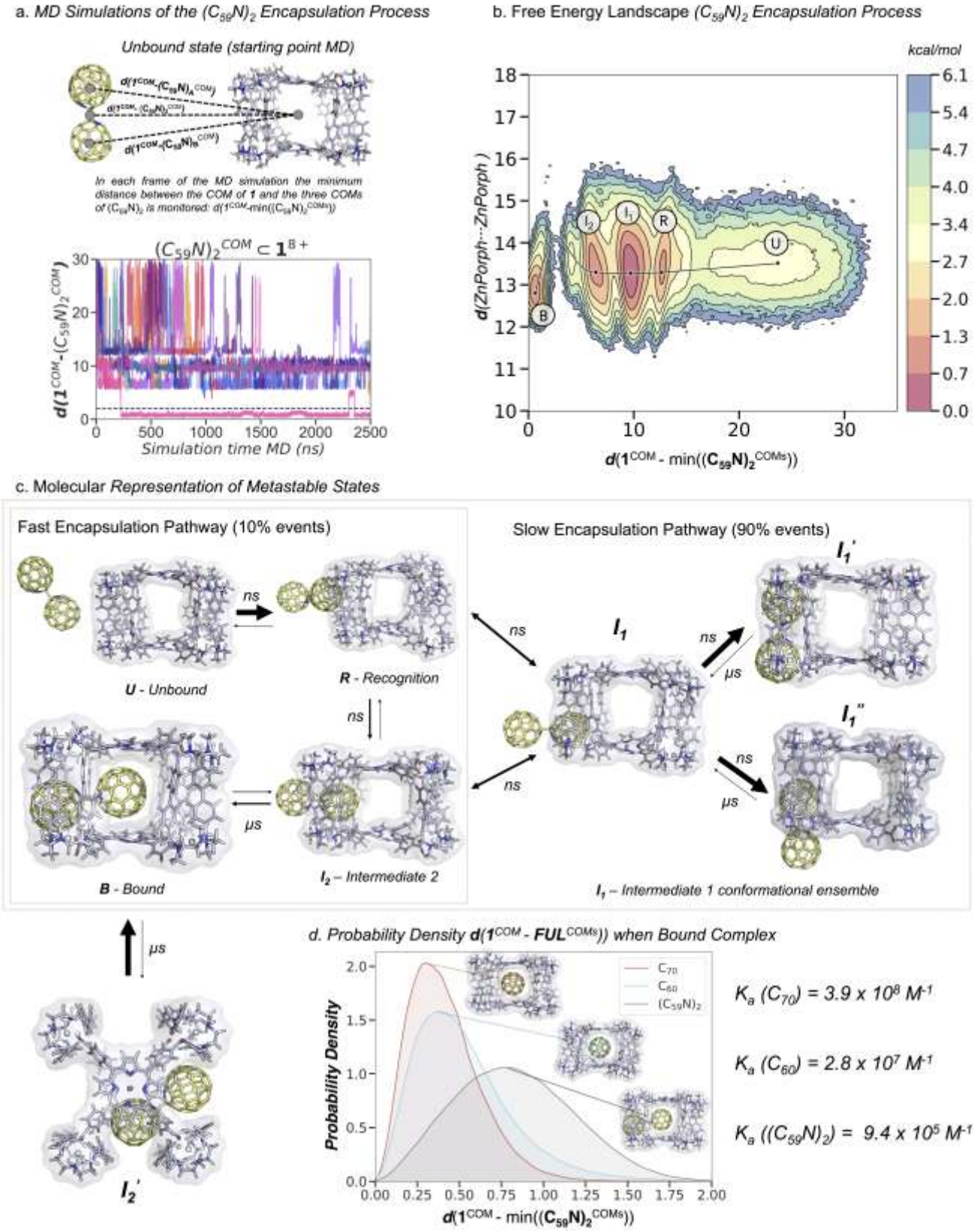

Figure 7. a) Plot of the distance between the center of masses of $(C_{59}N)_2$ and the supramolecular capsule, $d((\mathbf{1}^{COM}\text{-min}(C_{59}N)_2)^{COMs})$ for ten representative 2.5 μs replicas of MD simulations. Distances below 2 Å indicate complete C_{70} encapsulation (dashed horizontal line). Spontaneous binding is observed in one out of ten of the selected replicas. b) Reconstructed Free Energy Landscape (FEL) of the spontaneous encapsulation process of $(C_{59}N)_2$ obtained from an accumulated simulation time of 75 μs of MD simulations. The FEL has been reconstructed using $d(\text{min}(C_{59}N)_2{}^{COM}\text{-}\mathbf{1}^{COM})$ and ZnPorph···ZnPorph distances. c) Eight relevant metastable states are identified: Unbound (**U**), Recognition (**R**), Intermediate 1 (**I_1**), **I_1'**, **I_2"**, Intermediate 2 (**I_2**), **I_2'**, and Bound (**B**) states. Mo-

lecular representation of each state. The width of the arrow indicates the most frequent events observed. d) Probability density distribution for bound complexes with C_{60}, C_{70} and $(C_{59}N)_2$.

CONCLUSIONS

In summary, a synergy protocol combining ^{1}H-^{1}H exchange spectroscopy (EXSY) NMR and conventional and accelerated molecular dynamics (MD/aMD), has been presented for the in-depth study of the recognition and binding events occurring between coordination capsule $\mathbf{1}^{8+}$ and C_{60}/C_{70} fullerenes. In the long time-scale of exchange NMR experiments (ms), a similarly facile entrance (k'_{on}) of both C_{60} and C_{70} takes place, in contrast to the 10 times higher reluctance of C_{70} to be expelled (k_{off}) from the inner cavity. In addition, in the ns - μs time-scale accessible to the MD simulations (non-equilibrium regime), a number of key structural and interaction features have been revealed: a) the highly flexible and adaptable nature of the nanocapsule, b) the easy access of fullerenes towards the capsule inner space without disruption of the structure, c) the existence of a gate-located metastable state in which fullerenes are guided to the capsule interior, d) the exceptional stability of the fullerenes sandwiched in between the two porphyrins, and e) the role of the porphyrin phenyl rings for permitting the deep entrance and maintaining the fullerenes in the center of the cavity. This new methodology not only allows studying the unbounded-bounded host-guest adducts, but also understanding in molecular detail the factors governing recognition and binding of the guest identifying metastable states and multiple binding pathways key for the recognition process that were not observed in XRD and NMR experiments. The guest encapsulation process is tightly coupled and regulated by $\mathbf{1}^{8+}$ intrinsic dynamics. The predictability of the computational nanoreactor MD/aMD approach has been further confirmed with the C_{60}/C_{70} competition case study. Finally, the encapsulation of $(C_{59}N)_2$ in $\mathbf{1}^{8+}$ has been described, representing the first example reported of a supramolecular coordination host for the azafullerene. Computational predictions indicate that the encapsulation and the recognition pathway of azafullerene are hampered by the dynamic features of the supramolecular nanocapsule leading to slower binding. Probability density distribution of the bound states for C_{60}, C_{70} and $(C_{59}N)_2$ clearly indicate a higher mobility for $(C_{59}N)_2$, which is translated to a lower affinity measured association constant ($K_a = 9.4 \cdot 10^5$ M^{-1}) one and two order of magnitudes lower than the K_a reported for C_{60} and C_{70}, respectively.

At the molecular level, the nanocapsule displays dynamical features that resemble those typical of biomolecules including conformational selection of pre-existing states upon fullerene encapsulation and open-closed transitions to assist guest binding and exchange. The conformational heterogeneity displayed by this empty nanocapsule could have an immediate impact on efforts to design and engineer *de novo* nanocapsules for the purification of fullerene and endohedral metallofullerenes (EMFs) mixtures. We envision that this combined analysis approach might be extrapolated to a large number of supramolecular host-guest platforms for gaining a deeper mechanistic understanding of the dynamic events at a molecular level.

ASSOCIATED CONTENT

Supporting Information

The Supporting Information is available free of charge on the website.

AUTHOR INFORMATION

Corresponding Author

jjbarbero@cicbiogune.es
ferran.feixas@udg.edu
xavi.ribas@udg.edu

Notes

The authors declare no competing financial interest.

ACKNOWLEDGMENT

We acknowledge financial support from AEI and MINECO-Spain (projects CTQ2016-77989-P to X.R., RTI2018-101032-J-I00 to F.F., and RTI2018-094751-B-C21 and Severo Ochoa Excellence accreditation SEV-2016-0644 to J.J.B.), and from Generalitat de Catalunya for project 2017SGR264 (X.R.) and 2017SGR1707 (F.F). X.R. and M.C. also thank ICREA Acadèmia awards. F.F. thanks the European Community for MSCA-IF-2014-EF-661160-MetAccembly grant. A.G. also thanks Instituto de Salud Carlos III of Spain, ISCIII (grant PRB3 IPT17/0019)
The authors are grateful for the computer resources, technical expertise, and assistance provided by the Barcelona Supercomputing Center – Centro Nacional de Supercomputación.

REFERENCES

1. Houk, K. N.; Leach, A. G.; Kim, S. P.; Zhang, X., Binding Affinities of Host–Guest, Protein–Ligand, and Protein–Transition-State Complexes. *Angew. Chem. Int. Ed.* **2003,** *42*, 4872-4897.
2. Schreiber, G.; Haran, G.; Zhou, H. X., Fundamental Aspects of Protein−Protein Association Kinetics. *Chem. Rev.* **2009,** *109*, 839-860.
3. Bernetti, M.; Masetti, M.; Rocchia, W.; Cavalli, A., Kinetics of Drug Binding and Residence Time. *Ann. Rev. Phys. Chem.* **2019,** *70*, 143-171.
4. Boehr, D. D.; Nussinov, R.; Wright, P. E., The role of dynamic conformational ensembles in biomolecular recognition. *Nat. Chem. Biol.* **2009,** *5*, 789-796.
5. Pullen, S.; Clever, G. H., Mixed-Ligand Metal–Organic Frameworks and Heteroleptic Coordination Cages as Multifunctional Scaffolds—A Comparison. *Acc. Chem. Res.* **2018,** *51*, 3052-3064.
6. Rizzuto, F. J.; von Krbek, L. K. S.; Nitschke, J. R., Strategies for binding multiple guests in metal–organic cages. *Nat. Rev. Chem.* **2019,** *3*, 204-222.
7. Mukhopadhyay, R. D.; Kim, Y.; Koo, J.; Kim, K., Porphyrin Boxes. *Acc. Chem. Res.* **2018,** *51*, 2730-2738.
8. Davis, A. V.; Raymond, K. N., The Big Squeeze: Guest Exchange in an M4L6 Supramolecular Host. *J. Am. Chem. Soc.* **2005,** *127*, 7912-7919.

9. Komine, S.; Takahashi, S.; Kojima, T.; Sato, H.; Hiraoka, S., Self-Assembly Processes of Octahedron-Shaped Pd6L4 Cages. *J. Am. Chem. Soc.* **2019,** *141*, 3178-3186.
10. Krabbenborg, S. O.; Veerbeek, J.; Huskens, J., Spatially Controlled Out-of-Equilibrium Host–Guest System under Electrochemical Control. *Chem. Eur. J.* **2015,** *21*, 9638-9644.
11. Pesce, L.; Perego, C.; Grommet, A. B.; Klajn, R.; Pavan, G. M., Molecular Factors Controlling the Isomerization of Azobenzenes in the Cavity of a Flexible Coordination Cage. *J. Am. Chem. Soc.* **2020,** *142*, 9792-9802.
12. Orozco, M., A theoretical view of protein dynamics. *Chem. Soc. Rev.* **2014,** *43*, 5051-5066.
13. Dror, R. O.; Dirks, R. M.; Grossman, J. P.; Xu, H.; Shaw, D. E., Biomolecular Simulation: A Computational Microscope for Molecular Biology. *Annu. Rev. Biophys.* **2012,** *41*, 429-452.
14. Frederix, P. W. J. M.; Patmanidis, I.; Marrink, S. J., Molecular simulations of self-assembling bio-inspired supramolecular systems and their connection to experiments. *Chem. Soc. Rev.* **2018,** *47*, 3470-3489.
15. Davis, A. V.; Yeh, R. M.; Raymond, K. N., Supramolecular assembly dynamics. *PNAS* **2002,** *99*, 4793-4796.
16. Feixas, F.; Lindert, S.; Sinko, W.; McCammon, J. A., Exploring the role of receptor flexibility in structure-based drug discovery. *Biophys. Chem.* **2014,** *186*, 31-45.
17. Shan, Y.; Kim, E. T.; Eastwood, M. P.; Dror, R. O.; Seeliger, M. A.; Shaw, D. E., How Does a Drug Molecule Find Its Target Binding Site? *J. Am. Chem. Soc.* **2011,** *133*, 9181-9183.
18. Buch, I.; Giorgino, T.; De Fabritiis, G., Complete reconstruction of an enzyme-inhibitor binding process by molecular dynamics simulations. *PNAS* **2011,** *108*, 10184-10189.
19. Decherchi, S.; Berteotti, A.; Bottegoni, G.; Rocchia, W.; Cavalli, A., The ligand binding mechanism to purine nucleoside phosphorylase elucidated via molecular dynamics and machine learning. *Nat. Comm.* **2015,** *6*, 6155.
20. Dror, R. O.; Green, H. F.; Valant, C.; Borhani, D. W.; Valcourt, J. R.; Pan, A. C.; Arlow, D. H.; Canals, M.; Lane, J. R.; Rahmani, R.; Baell, J. B.; Sexton, P. M.; Christopoulos, A.; Shaw, D. E., Structural basis for modulation of a G-protein-coupled receptor by allosteric drugs. *Nature* **2013,** *503*, 295-299.
21. Lotz, S. D.; Dickson, A., Unbiased Molecular Dynamics of 11 min Timescale Drug Unbinding Reveals Transition State Stabilizing Interactions. *J. Am. Chem. Soc.* **2018,** *140*, 618-628.
22. Saglam, A. S.; Chong, L. T., Protein–protein binding pathways and calculations of rate constants using fully-continuous, explicit-solvent simulations. *Chem. Sci.* **2019,** *10*, 2360-2372.
23. Kollias, L.; Cantu, D. C.; Tubbs, M. A.; Rousseau, R.; Glezakou, V.-A.; Salvalaglio, M., Molecular Level Understanding of the Free Energy Landscape in Early Stages of Metal–Organic Framework Nucleation. *J. Am. Chem. Soc.* **2019,** *141*, 6073-6081.
24. Yoneya, M.; Yamaguchi, T.; Sato, S.; Fujita, M., Simulation of Metal–Ligand Self-Assembly into Spherical Complex M6L8. *J. Am. Chem. Soc.* **2012,** *134*, 14401-14407.
25. Barendt, T. A.; Myers, W. K.; Cornes, S. P.; Lebedeva, M. A.; Porfyrakis, K.; Marques, I.; Félix, V.; Beer, P. D., The green box: an electronically versatile perylene diimide macrocyclic host for fullerenes. *J. Am. Chem. Soc.* **2019**.
26. Pluth, M. D.; Raymond, K. N., Reversible guest exchange mechanisms in supramolecular host–guest assemblies. *Chem. Soc. Rev.* **2007,** *36*, 161-171.
27. Dixon, T.; Lotz, S. D.; Dickson, A., Predicting ligand binding affinity using on- and off-rates for the SAMPL6 SAMPLing challenge. *J. Comput. Aided Mol. Des.* **2018,** *32*, 1001-1012.
28. Shi, Y.; Cai, K.; Xiao, H.; Liu, Z.; Zhou, J.; Shen, D.; Qiu, Y.; Guo, Q.-H.; Stern, C.; Wasielewski, M. R.; Diederich, F.; Goddard, W. A.; Stoddart, J. F., Selective Extraction of C70 by a Tetragonal Prismatic Porphyrin Cage. *J. Am. Chem. Soc.* **2018,** *140*, 13835-13842.
29. Camacho Gonzalez, J.; Mondal, S.; Ocayo, F.; Guajardo-Maturana, R.; Muñoz-Castro, A., Nature of C60 and C70 fullerene encapsulation in a porphyrin- and metalloporphyrin-based cage: Insights from dispersion-corrected density functional theory calculations. *Int. J. Quantum Chem.* **2020,** *120*, e26080.
30. Fuertes-Espinosa, C.; García-Simón, C.; Pujals, M.; Garcia-Borràs, M.; Gómez, L.; Parella, T.; Juanhuix, J.; Imaz, I.; Maspoch, D.; Costas, M.; Ribas, X., Supramolecular Fullerene Sponges as Catalytic Masks for Regioselective Functionalization of C60. *Chem* **2020,** *6*, 169-186.
31. Rizzi, A.; Murkli, S.; McNeill, J. N.; Yao, W.; Sullivan, M.; Gilson, M. K.; Chiu, M. W.; Isaacs, L.; Gibb, B. C.; Mobley, D. L.; Chodera, J. D., Overview of the SAMPL6 host–guest binding affinity prediction challenge. *J. Comput. Aided Mol. Des.* **2018,** *32*, 937.
32. Slochower, D. R.; Henriksen, N. M.; Wang, L.-P.; Chodera, J. D.; Mobley, D. L.; Gilson, M. K., Binding Thermodynamics of Host–Guest Systems with SMIRNOFF99Frosst 1.0.5 from the Open Force Field Initiative. *J. Chem. Theory Comput.* **2019,** *15*, 6225-6242.
33. Schönherr, H.; Beulen, M. W. J.; Bügler, J.; Huskens, J.; van Veggel, F. C. J. M.; Reinhoudt, D. N.; Vancso, G. J., Individual Supramolecular Host−Guest Interactions Studied by Dynamic Single Molecule Force Spectroscopy. *J. Am. Chem. Soc.* **2000,** *122*, 4963-4967.
34. Zheng, X.; Wang, D.; Shuai, Z.; Zhang, X., Molecular Dynamics Simulations of the Supramolecular Assembly between an Azobenzene-Containing Surfactant and α-Cyclodextrin: Role of Photoisomerization. *J. Phys. Chem. B* **2012,** *116*, 823-832.
35. Young, T. A.; Martí-Centelles, V.; Wang, J.; Lusby, P. J.; Duarte, F., Rationalizing the Activity of an "Artificial Diels-Alderase": Establishing Efficient and Accurate Protocols for Calculating Supramolecular Catalysis. *J. Am. Chem. Soc.* **2020,** *142*, 1300-1310.
36. Norjmaa, G.; Maréchal, J.-D.; Ujaque, G., Microsolvation and Encapsulation Effects on Supramolecular Catalysis: C–C Reductive Elimination inside [Ga4L6]12– Metallocage. *J. Am. Chem. Soc.* **2019,** *141*, 13114-13123.
37. Pahima, E.; Zhang, Q.; Tiefenbacher, K.; Major, D. T., Discovering Monoterpene Catalysis Inside Nanocapsules with Multiscale Modeling and Experiments. *J. Am. Chem. Soc.* **2019,** *141*, 6234-6246.
38. Welborn, V. V.; Li, W.-L.; Head-Gordon, T., Interplay of water and a supramolecular capsule for catalysis of reductive elimination reaction from gold. *Nat. Comm.* **2020,** *11*, 415.

39. Betz, R. M.; Dror, R. O., How Effectively Can Adaptive Sampling Methods Capture Spontaneous Ligand Binding? *J. Chem. Theor. Comput.* **2019,** *15*, 2053-2063.
40. You, W.; Tang, Z.; Chang, C.-e. A., Potential Mean Force from Umbrella Sampling Simulations: What Can We Learn and What Is Missed? *J. Chem. Theor. Comput.* **2019,** *15*, 2433-2443.
41. Leonhard, A. C.; Whitmer, J. K., Accurate Determination of Cavitand Binding Free Energies via Unrestrained Advanced Sampling. *J. Chem. Theor. Comput.* **2019,** *15*, 5761-5768.
42. Hamelberg, D.; Mongan, J.; McCammon, J. A., Accelerated molecular dynamics: A promising and efficient simulation method for biomolecules. *J. Chem. Phys.* **2004,** *120*, 11919-11929.
43. Miao, Y.; Feixas, F.; Eun, C.; McCammon, J. A., Accelerated molecular dynamics simulations of protein folding. *J. Comput. Chem.* **2015,** *36*, 1536-1549.
44. Miao, Y.; McCammon, J. A., Graded activation and free energy landscapes of a muscarinic G-protein–coupled receptor. *PNAS* **2016,** *113*, 12162-12167.
45. Tomás-Loba, A.; Manieri, E.; González-Terán, B.; Mora, A.; Leiva-Vega, L.; Santamans, A. M.; Romero-Becerra, R.; Rodríguez, E.; Pintor-Chocano, A.; Feixas, F.; López, J. A.; Caballero, B.; Trakala, M.; Blanco, Ó.; Torres, J. L.; Hernández-Cosido, L.; Montalvo-Romeral, V.; Matesanz, N.; Roche-Molina, M.; Bernal, J. A.; Mischo, H.; León, M.; Caballero, A.; Miranda-Saavedra, D.; Ruiz-Cabello, J.; Nevzorova, Y. A.; Cubero, F. J.; Bravo, J.; Vázquez, J.; Malumbres, M.; Marcos, M.; Osuna, S.; Sabio, G., p38γ is essential for cell cycle progression and liver tumorigenesis. *Nature* **2019,** *568*, 557-560.
46. García-Simón, C.; Garcia-Borràs, M.; Gómez, L.; Parella, T.; Osuna, S.; Juanhuix, J.; Imaz, I.; Maspoch, D.; Costas, M.; Ribas, X., Sponge-like molecular cage for purification of fullerenes. *Nat. Commun.* **2014,** *5*, 5557.
47. Fuertes-Espinosa, C.; Gómez-Torres, A.; Morales-Martínez, R.; Rodríguez-Fortea, A.; García-Simón, C.; Gándara, F.; Imaz, I.; Juanhuix, J.; Maspoch, D.; Poblet, J. M.; Echegoyen, L.; Ribas, X., Purification of Uranium-based Endohedral Metallofullerenes (EMFs) by Selective Supramolecular Encapsulation and Release. *Angew. Chem. Int. Ed.* **2018,** *57*, 11294-11299.
48. Fuertes-Espinosa, C.; Murillo, J.; Soto, M. E.; Ceron, M. R.; Morales-Martínez, R.; Rodríguez-Fortea, A.; Poblet, J. M.; Echegoyen, L.; Ribas, X., Highly selective encapsulation and purification of U-based C78-EMFs within a supramolecular nanocapsule. *Nanoscale* **2019,** *11*, 23035-23041.
49. Hummelen, J. C.; Knight, B.; Pavlovich, J.; González, R.; Wudl, F., Isolation of the Heterofullerene C59N as Its Dimer (C59N)2. *Science* **1995,** *269*, 1554-1556.
50. Colomban, C.; Szalóki, G.; Allain, M.; Gómez, L.; Goeb, S.; Sallé, M.; Costas, M.; Ribas, X., Reversible C60 Ejection from a Metallocage through the Redox-Dependent Binding of a Competitive Guest. *Chem. Eur. J.* **2017,** *23*, 3016-3022.
51. Park, S. J.; Kwon, O.-H.; Lee, K.-S.; Yamaguchi, K.; Jang, D.-J.; Hong, J.-I., Dimeric Capsules with a Nanoscale Cavity for [60]Fullerene Encapsulation. *Chem. Eur. J.* **2008,** *14*, 5353-5359.
52. Jeener, J.; Meier, B. H.; Bachmann, P.; Ernst, R. R., Investigation of exchange processes by two-dimensional NMR spectroscopy. *J. Chem. Phys.* **1979,** *71*, 4546-4553.
53. Perrin, C. L.; Dwyer, T. J., Application of two-dimensional NMR to kinetics of chemical exchange. *Chem. Rev.* **1990,** *90*, 935-967.
54. Nakazawa, J.; Sakae, Y.; Aida, M.; Naruta, Y., Kinetic Investigations of the Process of Encapsulation of Small Hydrocarbons into a Cavitand−Porphyrin. *J. Org. Chem.* **2007,** *72*, 9448-9455.
55. Frunzi, M.; Baldwin, A. M.; Shibata, N.; Iwamatsu, S.-I.; Lawler, R. G.; Turro, N. J., Kinetics and Solvent-Dependent Thermodynamics of Water Capture by a Fullerene-Based Hydrophobic Nanocavity. *J. Chem. Phys. A* **2011,** *115*, 735-740.
56. Rizzuto, F. J.; Nitschke, J. R., Stereochemical plasticity modulates cooperative binding in a CoII12L6 cuboctahedron. *Nat. Chem.* **2017,** *9*, 903.
57. Schneemann, A.; Bon, V.; Schwedler, I.; Senkovska, I.; Kaskel, S.; Fischer, R. A., Flexible metal–organic frameworks. *Chem. Soc. Rev.* **2014,** *43*, 6062-6096.
58. Kovermann, M.; Grundström, C.; Sauer-Eriksson, A. E.; Sauer, U. H.; Wolf-Watz, M., Structural basis for ligand binding to an enzyme by a conformational selection pathway. *PNAS* **2017,** *114*, 6298-6303.
59. Miao, Y.; McCammon, J. A., Unconstrained enhanced sampling for free energy calculations of biomolecules: a review. *Mol. Simul.* **2016,** *42*, 1046-1055.
60. Iizumi, Y.; Okazaki, T.; Liu, Z.; Suenaga, K.; Nakanishi, T.; Iijima, S.; Rotas, G.; Tagmatarchis, N., Host–guest interactions in azafullerene (C59N)-single-wall carbon nanotube (SWCNT) peapod hybrid structures. *Chem. Commun.* **2010,** *46*, 1293-1295.
61. Rio, J.; Beeck, S.; Rotas, G.; Ahles, S.; Jacquemin, D.; Tagmatarchis, N.; Ewels, C.; Wegner, H. A., Electronic Communication between two [10]cycloparaphenylenes and Bis(azafullerene) (C59N)2 Induced by Cooperative Complexation. *Angew. Chem. Int. Ed.* **2018,** *57*, 6930-6934.
62. Stergiou, A.; Rio, J.; Griwatz, J. H.; Arčon, D.; Wegner, H. A.; Ewels, C. P.; Tagmatarchis, N., A Long-Lived Azafullerenyl Radical Stabilized by Supramolecular Shielding with a [10]Cycloparaphenylene. *Angew. Chem. Int. Ed.* **2019,** *58*, 17745-17750.

TOC (include azafullerene in TOC??)